Deep learning based brain tumor classification and detection system

Ali ARI[*], **Davut HANBAY**
Department of Computer Engineering, Faculty of Engineering, İnönü University, Malatya, Turkey

Abstract: The brain cancer treatment process depends on the physician's experience and knowledge. For this reason, using an automated tumor detection system is extremely important to aid radiologists and physicians to detect brain tumors. The proposed method has three stages, which are preprocessing, the extreme learning machine local receptive fields (ELM-LRF) based tumor classification, and image processing based tumor region extraction. At first, nonlocal means and local smoothing methods were used to remove possible noises. In the second stage, cranial magnetic resonance (MR) images were classified as benign or malignant by using ELM-LRF. In the third stage, the tumors were segmented. The purpose of the study was using only cranial MR images, which have a mass, in order to save the physician's time. In the experimental studies the classification accuracy of cranial MR images is 97.18%. Evaluated results showed that the proposed method's performance was better than the other recent studies in the literature. Experimental results also proved that the proposed method is effective and can be used in computer aided brain tumor detection.

Key words: Brain tumor detection, deep learning, extreme learning machine, local receptive fields

1. Introduction

The brain is the management center of the central nervous system and is responsible for the execution of activities all throughout the human body. Brain tumors can threaten human life directly. If the tumor is detected at an early stage, the patient's survival chance increases. Magnetic resonance (MR) imaging is widely used by physicians in order to determine the existence of tumors or the specification of the tumors [1]. The qualification of the brain cancer treatment depends on the physician's experience and knowledge [2]. For this reason, using an automated and flawless working tumor detection system is extremely important to aid physicians to detect brain tumors. Detection of tumors in the brain via MR images has become an important task and numerous studies have been conducted in recent years. A hybrid fuzzy c-means clustering algorithm and a cellular automata-based brain tumor segmentation method were presented in [3]. The authors used a gray level cooccurrence matrix (GLCM) and a new similarity function based solution for seed growing problems in traditional segmentation algorithms. For performance evaluation, they used the BraTS2013 dataset. A fully automated brain tumor detecting method was proposed in [4]. Their method had five stages, which were image acquisition, preprocessing, segmentation, tumor extraction, and evaluation. Tumor extraction was performed by area and circularity features. This method's performance was compared with the (ground truth) manually segmented tumors. Average Dice coefficient was 0.729. A semiautomatic technique for MR brain image segmentation was presented in [5]. This segmentation technique was composed of MR image information that was beyond human perception in order to develop a fused feature map. The obtained feature map was

---

[*]Correspondence: ali.ari@inonu.edu.tr

used as a stopping function for the initialized curve in the framework of an active contour model to obtain a well-segmented region of interest. The results were compared with manually segmented images by using Jaccard's coefficient and overlap index parameters. In [6] a multistage approach was presented to perform tumor detection in MR images. The first step of this approach was preprocessing, which included noise filtering, image cropping, scaling, and histogram equalization. Feature extraction was then performed by using GLCM, gray level run length matrix (GLRLM), and histogram based techniques. The random forest classifier was used as a classifier. At the end of the study, tumor detection was performed using fast bounding box and tumor segmentation by using an active contour model. A total of 120 patient's data were used to evaluate model performance. The classification accuracy of their model was 87.62%. In [7] a wavelet based method was applied to MR imaging to extract a feature vector. The extracted feature vector was called the modality fusion vector (MFV). A Markov random field model was used for segmentation of MR images. In [8], brain tumor detection in 3D images was performed automatically. Histogram matching and bias field correction were used. The region of interest was separated from the background. The random forest method was used for segmentation of the tumors. Local binary pattern in three orthogonal planes (LBP-TOP) and histogram of orientation gradients (HOG-TOP) of MR images were used as to the classifier. The performance was tested by the brain tumor segmentation (BRATS) 2013 dataset. A deep learning such as convolutional neural network (CNN) technique based classification of computed tomography (CT) brain images was presented in [9]. The application of deep learning CNN to the classification of CT brain images was presented in [10,11], where the authors proposed a multiple CNN framework with discrimination mechanism which is effective to achieve these goals. The authors initially constructed a different triplanar 2D CNN architecture for 3D voxel classification, which greatly reduced the segmentation time. The BRATS 2013 dataset was used for both training and testing. In [1], an automatic segmentation method based on CNN exploring small 3×3 kernels was presented. The proposed method was tested using the BRATS 2013 dataset. In [12], emphasis was placed on the latest trend of deep learning techniques in this area. State-of-the-art algorithms, with an emphasis on deep learning methods, were argued. CNN architecture has been used for the classification of brain tumors. The CNN aims to use the spatial information between the input image pixels using two basic processes, known as convolution and pooling. These processes run on the background and consecutive layers of the network. The features obtained by the convolution and roundup operations increase classification success. The major disadvantage of CNN is that the training period is long and there are problems with being able to stick to a single solution during training [13]. Extreme learning machine (ELM) is a method of classification that has been used in studies for recent years, and which has been proposed to overcome some of the disadvantages of the backpropagation algorithm [14]. ELM has significant advantages such as the speed of learning process and less complexity. The structure of ELM-LRF, in which LRF information is integrated into the ELM, has been proposed as an alternative model to the CNN [15].

The paper is organized as follows: theoretical background is given in Section 2, proposed method is described in Section 3, experimental results and discussions are given in Section 4, and finally a conclusion is given in Section 5.

2. Background

2.1. Convolutional neural network

CNN is a kind of multilayered feedforward (MLF) artificial neural network (or multilayered sensor), originally inspired by the visual cortex [16]. CNN is one of the important concepts of deep learning. CNN is generally

used in image recognition applications and it contains two basic processes, known as convolution and pooling. Until having high level classification accuracy, convolution and pooling layers are arranged. In addition, some feature maps can be found in each convolutional layer and weights of convolutional nodes in the same map are shared. These arrangements allow for the learning of different characteristics of the network while keeping the number of traceable parameters. CNN has fewer specific tasks compared to traditional methods and learns to extract features completely. The CNN process scheme is illustrated in Figure 1.
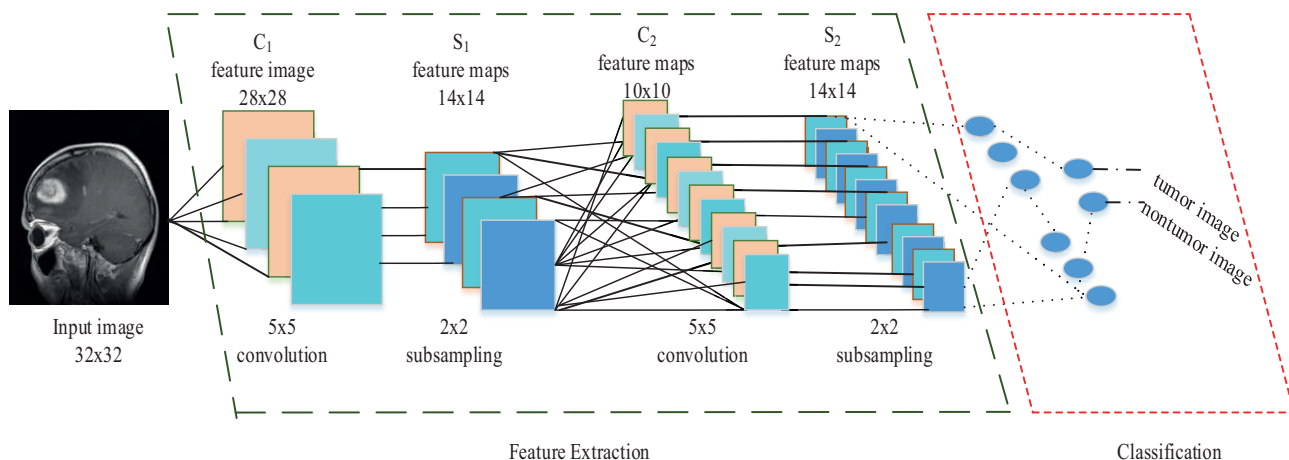

Figure 1. CNN process scheme.

2.2. Extreme learning machine

As illustrated in Figure 2, the ELM was designed by Huang et al. [17]. ELM is a single hidden layered feedforward neural network whose input weights are calculated randomly and output weights are calculated analytically [18].
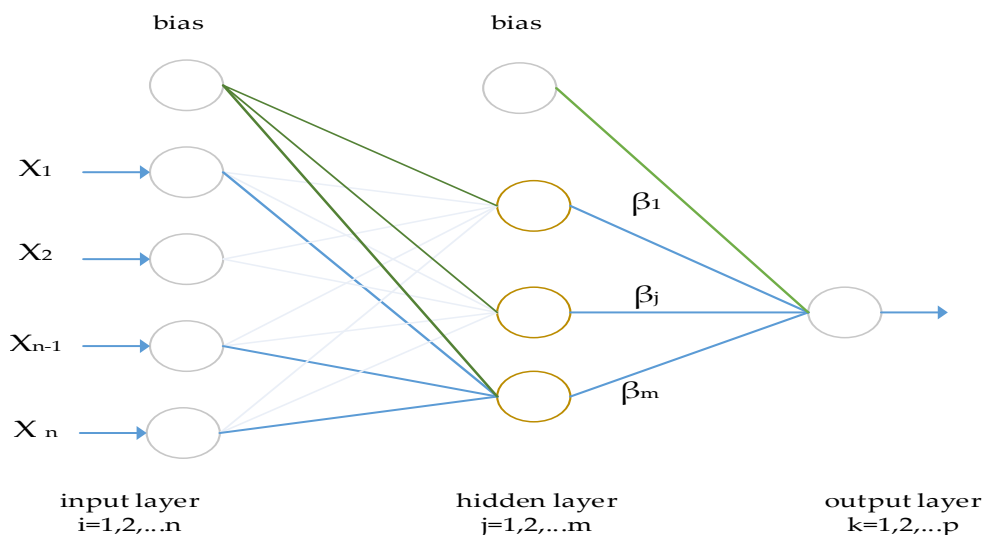

Figure 2. Single hidden layered feedforwarded neural network.

Activation functions such as sigmoidal, Gaussian, and hard-limited are used in the ELM hidden layer, while a linear function is used in the output layer. Besides its fast learning ability, ELM has a better

generalization success compared to feedforward networks that learn via backpropagation algorithm. ELM's learning algorithm is described in [13]. The input–output relationships are learned by ELM. The input x_i is represented as $x_i = [x_{i1}, x_{i2}, \ldots, x_{in}]^T \in R^n$ and the output t_i is represented as $t_i = [t_{i1}, t_{i2}, \ldots, t_{in}]^T \in R^m$. The single hidden layer feedforward network model has $\tilde{N}$ cells in the hidden layer, and $g(x)$ is the activation function modeled mathematically as in Eq. (1):

$$\sum_{i=1}^{\tilde{N}} \beta_i g\left(w_i x_j + b_i\right) = o_j, \qquad j = 1, \ldots, N, \tag{1}$$

where $w_i = [w_{i1}, w_{i2}, \ldots, w_{in}]^T$ is the weight vector between i hidden layer cells and input cells. On the other hand, $\beta_i = [\beta_{i1}, \beta_{i2}, \ldots, \beta_{im}]^T$ is a weight vector depending on i hidden layer cells and output cells. b_i is the ith hidden cells' threshold value. $w_i.x_j$ refers to the inner multiplication of w_i and x_j. The standard single hidden layered feedforwarded network model, which has $\tilde{N}$ hidden cells with $g(x)$ activation function, can reach zero mistakes. The relation between $\sum_{j=1}^{\tilde{N}} \|o_j - t_j\| = 0$, β_i, w_i, and b_i is given in Eq. (2).

$$\sum_{i=1}^{\tilde{N}} \beta_i g\left(w_i x_j + b_i\right) = t_j, \qquad j = 1, \ldots, N \tag{2}$$

N equalities given in Eq. (2) can be abbreviated as in Eq. (3),

$$H\beta = T \tag{3}$$

Here,

$$H = \begin{bmatrix} g\left(w_1.x_1 + b_1\right) & \cdots & g\left(w_{\tilde{N}}.x_1 + b_{\tilde{N}}\right) \\ \vdots & \cdots & \vdots \\ g\left(w_1.x_N + b_1\right) & \cdots & g\left(w_{\tilde{N}}.x_N + b_{\tilde{N}}\right) \end{bmatrix}_{Nx\tilde{N}}, \tag{4}$$

$$\beta = \begin{bmatrix} \beta_1^T \\ \vdots \\ \beta_{\tilde{N}}^T \end{bmatrix}_{\tilde{N}xm} \quad \text{and} \quad T = \begin{bmatrix} t_1^T \\ \vdots \\ t_N^T \end{bmatrix}_{Nxm}. \tag{5}$$

The output matrix of the hidden layer is called H.

2.3. Local receptive field extreme learning machine

Being a new deep learning concept, ELM-LRF covers two separate structures in its body [14]. The first of these structures has convolution and pooling. Square/square root techniques are used for the pooling. The second is the analytical calculation of β via the least squares technique. The structure of ELM-LRF is given in Figure 3.

First Structure: No learning activity takes place in this part; in other words, no weight updating is calculated. K is convolution filters' coefficients that are picked randomly at the beginning. If the size of the input image, whose features are to be extracted, is $d\,x\,d$ and convolution filter size is $r\,x\,r$, after the convolution

layer a $(d - r + 1)$ x $(d - r + 1)$ x K sized feature map can be obtained. In the convolution layer, given window sized features are acquired [14].

Second Structure: The extracted features from the input images, which belong to training set, are acquired via combining these features on a matrix. In this structure, the weight vector β, which is between the ELM's hidden layer and output layer, must be calculated analytically. In other words, the previously obtained matrix is accepted as $H \in R^{Nx(d-r+1)^2}$ matrix and β can be calculated analytically as in Eq. (6) [14].

$$\beta = \begin{cases} H^T \left(\frac{I}{C} + HH^T \right)^{-1} T & \text{if } N \leq K.(d-r+1)^2 \\ \left(\frac{I}{C} + HH^T \right)^{-1} H^T T & \text{if } N > K.(d-r+1)^2 \end{cases} \tag{6}$$

Here T represents the class of training data, I is the unit matrix, and C is the regulation coefficient.
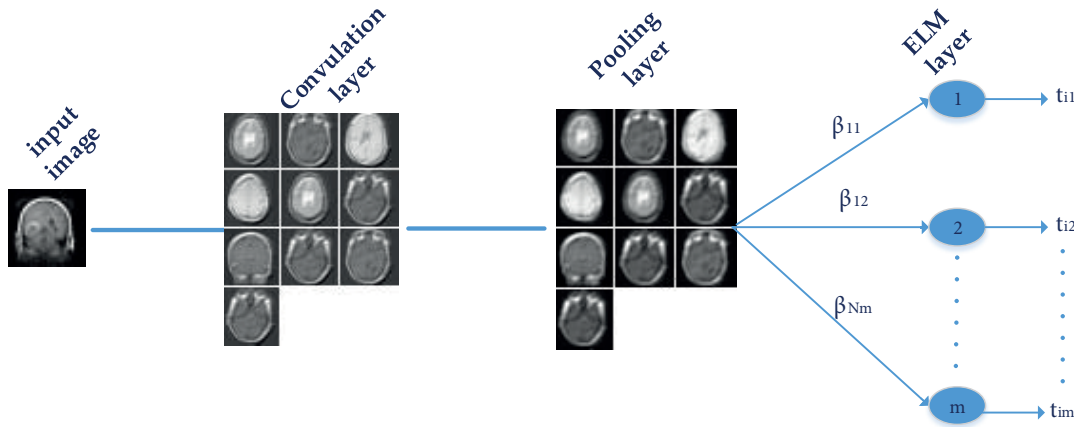

Figure 3. Structure of ELM-LRF.

2.4. Background of tumor detection

2.4.1. Preprocessing

MR images can be affected by various noise sources. Compressing images or transferring image data may also be a cause of noise. In this study, in order to reduce the noise, nonlocal means and local smoothing methods were used [19]. Some important structures and details in an image can behave like noise; these important details may also be removed. In Figure 4, column 1 represents axial plane MR images, column 2 shows coronal plane images and column 3 represents sagittal plane images. A sample original image is shown in Figure 4a and a preprocessed image is shown in Figure 4b.

2.4.2. Watershed segmentation and morphological process

A watershed segmentation technique was used for the effective segmentation of cranial MRIs. This technique was used for determination of tumors [20]. Watershed built on the terms of watershed lines is connected to topography and water source basin. By taking advantage of the topological structure of the object within an image, it processes the gray values and defines the object's borders ....[21]. Watershed transformation's algorithmic definition, which is based on submerge analogy, was upgraded by Vincent and Soille [21]. I is a

gray level image, and $h_{\min}$ and $h_{\max}$ are I's lowest and highest values. Recursion is identified via the h gray level changing from $h_{\min}$ to $h_{\max}$. At the beginning of recursion X_h basin cluster was counted as equal to dot clusters that have $h_{\min}$ value. Afterwards, X_h basin cluster's influence area in the threshold cluster widens consecutively [22,23].

$$X_h = \min_{h+1} \cup IZ_{T_{h+1}(f)}(X_h), \forall h \in [h_{\min}, h_{\max} - 1] \tag{7}$$

Gradient info is gathered as the first step of the watershed algorithm. This info is calculated by differentiating the first derivate of the change between pixel values. In the next stage, the sign is needed to initiate. For segmentation of an image, different pointer pixels belonging to each aimed class are needed. These pixels' location and quantity directly affects segmentation success. Watershed transformation has interesting features that are useful during image segmentation applications in mathematical morphology. This transformation is heuristically easy to comprehend. It produces fast results in the form of closed curves. However, it has disadvantages such as excessive segmentation. In this study, in order to avoid excessive segmentation, pointers were gathered initially by the assistance of morphological operators and then the watershed algorithm was applied to the image that includes pointers.

Opening Process: Objects in the image and gaps among them are cleaned according to the size of the structural element. Objects that stay on the upper side of the image shrink compared to the size of their original image. The objects were divided via the opening process with little damage to the image.

Closing Process: Dots in the image are close to each other at the end of closing process. Main lines were filled out. As in the expansion process, dots that were close to each other united and gaps between them were filled. The segmented skull image excludes data from MR images with the help of the watershed segmentation technique, as shown in Figure 4c. Afterwards, the soft tissue of the brain was obtained by extracting the skull image from the real image, as shown in Figure 4d. Detection of the tumor was conducted by morphological procedures and suitable threshold values, as shown in Figure 4e.

2.5. Dataset

The data used in this study were taken from [24]. In the dataset, images are in Digital Imaging and Communications in Medicine (DICOM) file format. Used benign and malignant tumor images belonging to each axial, coronal, and sagittal plane were digitized at 256×256. Sixteen patients' data were used. Nine patients' images were used for training and 7 patients' images were used for testing. All of the program's codes were written in MATLAB 2015 (The MathWorks Inc., Natick, MA, USA).

3. Proposed method

As illustrated in Figure 5, the proposed method was composed of three main stages: preprocessing, image classification with ELM-LRF, and tumor extraction based on image processing techniques. In the preprocessing stage, denoising and normalization operations were employed in order to prepare the input images for the next stage. In the classification stage, the ELM-LRF was used. Brain tumors were classified as benign or malignant. Convolution and pooling operations were applied to the images in the input layer. The input layer weights were selected randomly. The weights between the hidden layer and the output layer were calculated analytically by using the least square method. Watershed segmentation was used to detect tumors.
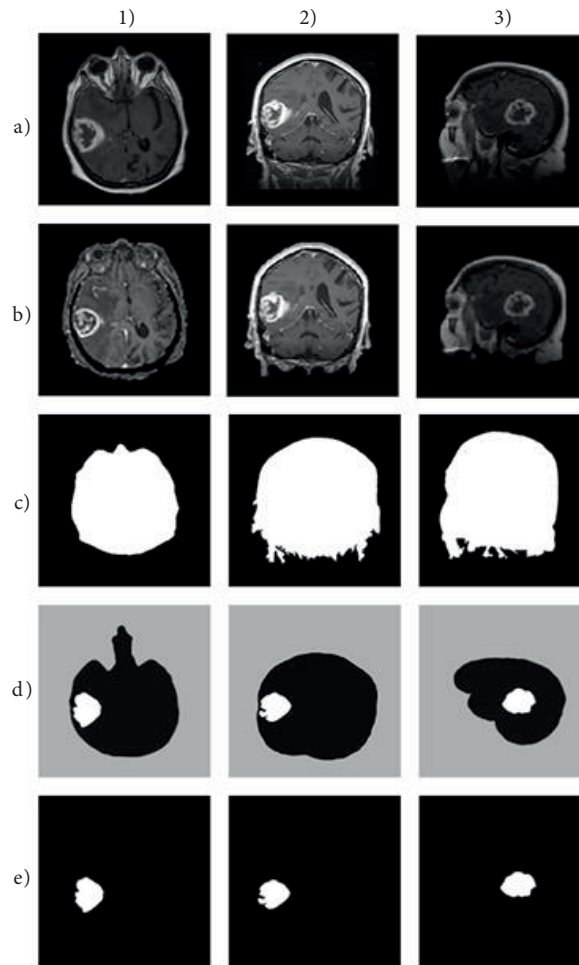
Figure 4. (a) Original image, (b) preprocessed image, (c) segmented skull image, (d) brain tissue extraction, (e) tumor detection.

4. Experimental results and discussion

All input images were resized to 32×32 before feeding into the ELM-LRF. ELM-LRF has four tunable parameters: convolution filter size r, convolution filter number K, pooling size, and C regulation coefficient. Based on the extensive experiments, the convolution filter size was determined as 5, the K value was chosen as 16, and the pooling size was chosen as 3. In addition, for identifying the most appropriate C value, an interval search was performed among $2^{-10}, 2^{-8}, \ldots, 2^8, 2^{10}$ and the C value with the minimum fault was chosen. Convolution and pooling process results are shown in Figure 6 and Figure 7, respectively.

The used CNN model for comparison has six layers. The first layer is the input layer. The second layer is the convolution layer following the input layer, where six convolution filters are used. The third layer is the pooling layer that was employed after the first convolution layer. Half sampling is employed in the pooling layer. The fourth layer is another convolution layer where 12 convolution filters are used. There is another pooling layer after the fourth convolution layer. The last layer is a fully connected layer. The sigmoid activation function is used at the CNN model.

In ELM-LRF, CNN, and Alexnet studies, all features were extracted directly from all images but in
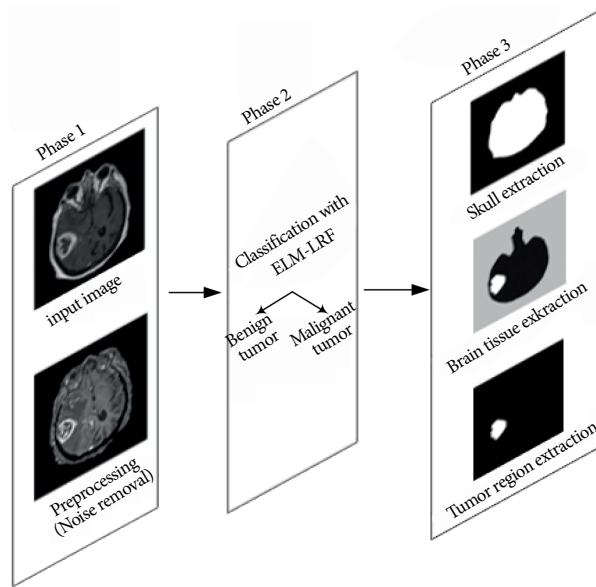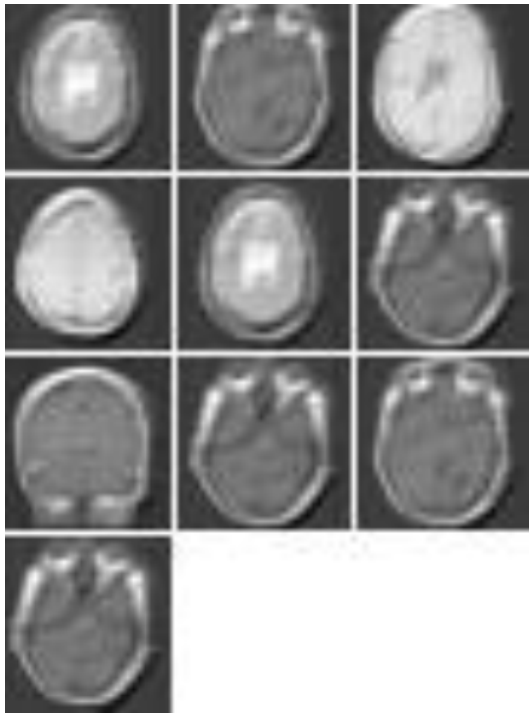
Figure 5. Proposed method.

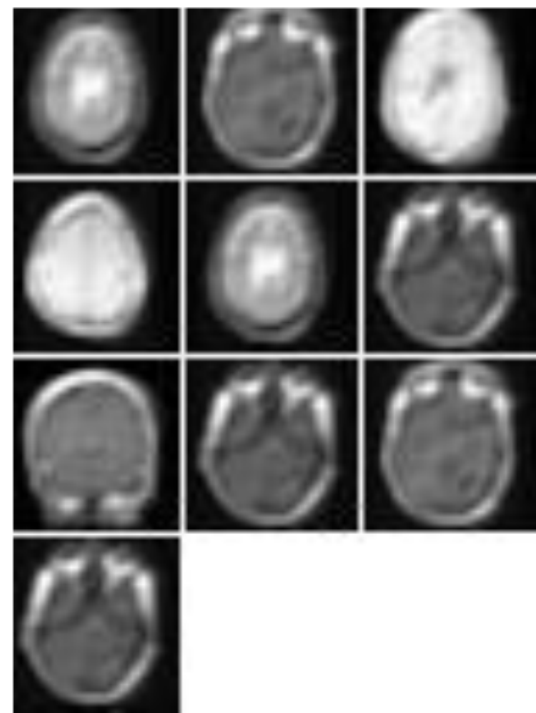**Figure 6**. Result of convolution operation.

Figure 7. Result of pooling operation.

Gabor wavelet transform and statistical based studies, all features were extracted from the tumor or tumor-like portion. In [25], the Gabor wavelet features and statistical features were extracted using Gabor wavelet transform, first-order statistical descriptors, GLCM, GLRLM, HOG, and LBP methods. Several classification methods such as support vector machine (SVM), K nearest neighbor (KNN), and neural network (NN) were applied for performance evaluation. For the comparison of the existing methods in [25] and the proposed

method, the same dataset was used. Table 1 shows the results of SVM with linear kernel, KNN, and NN for Gabor wavelet and statistical features extracted from T1-w images.

Table 1. Comparison of various classifiers on Gabor-wavelet and statistical features.

	SVM linear	KNN (k = 7)	NN
Gabor-wavelet features	$92.43 \pm 0.3\%$	$90.62 \pm 0.4\%$	$93.65 \pm 0.4\%$
Statistical features	$95.06 \pm 0.6\%$	$93.71 \pm 0.8\%$	$96.24 \pm 0.8\%$

The performances of four different methods are further compared: Gabor wavelets-based method, statistical features-based method, CNN, and ELM-LRF. The obtained results are given in Table 2. As seen in Table 2, 97.18% classification accuracy is obtained with the proposed method. The second-best performance is obtained by CNN (96.45%). Statistical features-based method and Gabor-wavelet features-based method yielded accuracy values of 96.24% and 93.65%, respectively. Thus, it can be concluded that deep learning-based methods outperform the methods compared.

Table 2. Performance comparison of various methods.

Methods	Classification success
ELM-LRF	97.18%
CNN	96.45%
Statistical features	96.24%
Gabor-wavelet features	93.65%

The performance of the compared results is further evaluated by calculating the sensitivity and specificity values, which can be defined as:

$$Sensitivity = \frac{TP}{TP + FN} * 100, \tag{8}$$

$$\text{Specificity} = \frac{TN}{TN + FP} * 100, \tag{9}$$

where *TP* is the number of true positives, *TN* is the number of true negatives, *FP* is the number of false positives, and *FN* denotes the number of false negatives. Malignant tumors are denoted as positive and benign tumors are denoted as negative. The calculated sensitivity and specificity values are given in Table 3. As seen, 96.80% sensitivity and 97.12% specificity values were calculated for the ELM-LRF method. These values are greater than those achieved with the other methods.

Table 3. Calculated sensitivity and specificity values.

Methods	Sensitivity	Specificity
ELM-LRF	96.80%	97.12%
CNN	96.23%	95.92%
Statistical features	96.15%	96.45%
Gabor-wavelet features	92.88%	93.15%

Table 4. Performance comparison of various methods.

Methods	Classification success
ELM-LRF	97.18%
AlexNet	96.91%

The ELM/LRF structure was also compared with AlexNet, which is well-known deep neural network structure. Classification performances are compared in Table 4. The CNN model has 5 convolutional layers and 3 fully connected layers. The first convolution layer employs 64 filters of size 11 × 11. The convolution stride was 4 pixels. Rectification linear unit (RELU) and local response normalization layers follow the first and second convolution layers. There were 5 max pooling layers in the architecture, which follow some of the convolution layers. The pooling operation was performed over a 3 × 3 pixel window, with stride 2. The second convolution layer filters the output of the previous layer by using 256 filters. These filters' size was 5 × 5. The convolution stride was 1 pixel and spatial padding was 2 pixels. The third convolutional layer also employs 256 filters. These filters' size was 3 × 3. The convolution stride and spatial padding is 1 pixel. There is only a RELU layer, which follows the third convolutional layer. The fourth and fifth convolutional layers have the same structure of the third convolutional layer. As we mentioned earlier, three fully connected layers follow the convolutional layers. All fully connected layers have 4096 channels. There are two dropout layers, which come after first and second fully connected layers, with probability of 0.5. Finally, a loss layer was used in the last layer.

5. Conclusion

In this study, the classification of cranial MR images and the detection of tumors in the brain were performed with the structure of ELM-LRF. This method is quite simple and useful when compared to ELM. The training period is short because it does not require any iteration. ELM-LRF is more efficient as the connections and the input weights are both randomly generated. The raw input directly applies to the network for learning of spatial correlations in natural images. ELM-RLF has four tunable parameters: convolution filter size r, convolution filter number K, pooling size, and the regulation coefficient C. Based on the extensive experiments, the convolution filter size was set to 5, the K value was chosen 16, and the pooling size was chosen 3. In addition, for identifying the most appropriate C value, an interval search was performed among 2^{-10}, 2^{-8}, …, 2^8, 2^{10} and the C value with the minimum fault was selected. The performance of the ELM-LRF was tested and also compared with two popular intelligent methods that are available in the literature. Classification accuracy of 97.18% was obtained with the proposed ELM-LRF method. As a result of this study the ELM-LRF structure is an important tool that can be used in biomedical image processing applications.

References

[1] Pereira S, Pinto A, Alves V, Silva CA. Brain tumor segmentation using convolutional neural networks in MRI images. IEEE T Med Imaging 2016; 35: 1240-1251.

[2] Dandıl E, Çakıroğlu M, Ekşi Z. Computer-aided diagnosis of malign and benign brain tumors on MR images. In: ICT Innovations 2014; 18-23 September 2017; Skopje, Macedonia. pp. 157-166.

[3] Sompong C, Wongthanavasu S. Brain tumor segmentation using cellular automata-based fuzzy c-means. In: 13th International Joint Conference on Computer Science and Software Engineering (JCSSE); 13-15 July 2016; Khon Kaen, Thailand. pp. 1-6.

[4] Sehgal A, Goel S, Mangipudi P, Mehra A, Tyagi D. Automatic brain tumor segmentation and extraction in MR images. In: Conference on Advances in Signal Processing (CASP); 9-11 June 2016; Pune, India. pp. 104-107.

[5] Banday SA, Mir AH. Statistical textural feature and deformable model based MR brain tumor segmentation. In: 6th International Conference on Advances in Computing, Communications and Informatics (ICACCI); 21-24 September 2016; Jaipur, India. pp. 657-663.

[6] Praveen GB, Agrawal A. Multi stage classification and segmentation of brain tumor. In: 3rd International Conference on Computing for Sustainable Global Development (INDIACom); 16-18 March 2016; New Delhi, India. pp. 1628-1632.

[7] Ahmadvand A, Kabiri P. Multispectral MRI image segmentation using Markov random field model. Signal, Image and Video Processing 2016; 10: 251-258.

[8] Abbasi S, Tajeripour F. Detection of brain tumor in 3D MRI images using local binary patterns and histogram orientation gradient. Neurocomputing 2017; 219: 526-535.

[9] Gao XW, Hui R. A deep learning based approach to classification of CT brain images. In: SAI Computing Conference (SAI); 13-15 July 2016; London, UK. pp. 28-31.

[10] Gao XW, Hui R, Tian Z. Classification of CT brain images based on deep learning networks. Comput Meth Prog Bio 2017; 138: 49-56.

[11] Zhao L, Jia K. Deep feature learning with discrimination mechanism for brain tumor segmentation and diagnosis. In: International Conference on Intelligent Information Hiding and Multimedia Signal Processing (IIH-MSP); 23-25 September 2015; Adelaide, Australia. pp. 306-309.

[12] Işın A, Direkoğlu C, Şah M. Review of MRI-based brain tumor image segmentation using deep learning methods. Procedia Comput Sci 2016; 102: 317-324.

[13] Arı B, Şengür A, Arı A. Local receptive fields extreme learning machine for apricot leaf recognition. In: International Conference on Artificial Intelligence and Data Processing (IDAP16); 17-18 September 2016; Malatya, Turkey. pp. 532-535.

[14] Huang GB, Zhu QY, Siew CK. Extreme learning machine: theory and applications. Neurocomputing 2006; 70: 489-501.

[15] Huang GB, Bai Z, Kasun LLC, Vong CM. Local receptive fields based extreme learning machine. IEEE Comput Intell M 2015; 10: 18-29.

[16] Han X, Li Y. The application of convolution neural networks in handwritten numeral recognition. International Journal of Database Theory and Application 2015; 8: 367-376.

[17] Tian H, Meng B, Wang S. Day-ahead electricity price prediction based on multiple ELM. In: Chinese Control and Decision Conference; 26-28 May 2010; Xuzhou, China. pp. 241-244.

[18] Deng W, Zheng Q, Chen L. Real-time collaborative filtering using extreme learning machine. In: IEEE/WIC/ACM International Joint Conference on Web Intelligence and Intelligent Agent Technology; 15-18 September 2009; Milan, Italy. pp. 466-473.

[19] Buades A, Coll B, More JM. A non-local algorithm for image denoising. In: 2005 IEEE Computer Society Conference on Computer Vision and Pattern Recognition (CVPR); 20-25 June 2005; San Diego, USA.

[20] Kaya H, Çavuşoğlu A, Çakmak HB, Şen, B, Delen D. Görüntü bölütleme ve görüntü benzetimi yöntemleri yardımı ile hastalığın teşhis ve tedavi sonrasi süreçlerinin desteklenmesi: Keratokonus örneği. Journal of the Faculty of Engineering and Architecture of Gazi University; 2016; 31: 737-747 (in Turkish).

[21] Beucher S. Mathematical morphology and geology: when image analysis uses the vocabulary of earth science a review of some applications. In: Geovision; 6-7 May 1999; University of Liège, Belgium. pp. 13-16.

[22] Lefèvre S. Knowledge from markers in watershed segmentation. In: International Conference on Computer Analysis of Images and Patterns; 22-24 August 2017; Ystad, Sweden. pp. 579-586.

[23] Topaloğlu M, Gangal A. Watershed dönüşümü kullanilarak corpus callosumun bölütlenmesi. In: URSI 3. Bilimsel Kongresi; 2006; Ankara, Turkey. pp. 607-609 (in Turkish).

[24] Kwan RKS, Evans AC, Pike GB. MRI simulation-based evaluation of image-processing and classification methods. IEEE T Med Imaging 1999; 18: 1085-1097.

[25] Nabizadeh N, Kubat M. Brain tumors detection and segmentation in MR images: Gabor wavelet vs. statistical features. Computers & Electrical Engineering 2015; 45: 286-301.